Altered Middle Lamella Homogalacturonan and Disrupted Deposition of (1→5)-α-L-Arabinan in the Pericarp of *Cnr*, a Ripening Mutant of Tomato[1]

Caroline Orfila, Graham B. Seymour, William G.T. Willats, I. Max Huxham, Michael C. Jarvis, Colin J. Dover, Andrew J. Thompson, and J. Paul Knox*

Centre for Plant Sciences, University of Leeds, Leeds LS2 9JT, United Kingdom (C.O., W.G.T.W., J.P.K.); Horticulture Research International, Wellesbourne, Warwick CV35 9EF, United Kingdom (G.B.S., A.J.T.); Cell and Molecular Biology Division, Institute of Biomedical and Life Sciences (I.M.H.) and Department of Chemistry (M.C.J.), University of Glasgow, Glasgow G12 8QQ, United Kingdom; and Horticulture Research International, East Malling, West Malling, Kent ME19 6BJ, United Kingdom (C.J.D.)

Cnr (colorless non-ripening) is a pleiotropic tomato (*Lycopersicon esculentum*) fruit ripening mutant with altered tissue properties including weaker cell-to-cell contacts in the pericarp (A.J. Thompson, M. Tor, C.S. Barry, J. Vrebalov, C. Orfila, M.C. Jarvis, J.J. Giovannoni, D. Grierson, G.B. Seymour [1999] Plant Physiol 120: 383–390). Whereas the genetic basis of the *Cnr* mutation is being identified by molecular analyses, here we report the identification of cell biological factors underlying the *Cnr* texture phenotype. In comparison with wild type, ripe-stage *Cnr* fruits have stronger, non-swollen cell walls (CW) throughout the pericarp and extensive intercellular space in the inner pericarp. Using electron energy loss spectroscopy imaging of calcium-binding capacity and anti-homogalacturonan (HG) antibody probes (PAM1 and JIM5) we demonstrate that maturation processes involving middle lamella HG are altered in *Cnr* fruit, resulting in the absence or a low level of HG-/calcium-based cell adhesion. We also demonstrate that the deposition of (1→5)-α-L-arabinan is disrupted in *Cnr* pericarp CW and that this disruption occurs prior to fruit ripening. The relationship between the disruption of (1→5)-α-L-arabinan deposition in pericarp CW and the *Cnr* phenotype is discussed.

The modification of cell walls (CW) is an important aspect of plant cell development. During fruit ripening the regulated swelling and dissolution of primary CW and the modification of middle lamellae (ML) between adherent primary CW are important factors contributing to tissue softening (Brady, 1987; Fischer and Bennett, 1991). The biochemistry and the spatial regulation of the dissolution of primary CW and ML are not fully understood, but in all cases appear to involve modifications to the network of pectic polysaccharides.

The multi-functional pectic polysaccharides are the most complex class of polysaccharides in primary plant CW (Jarvis, 1984). Core backbone structures of contiguous 1,4-linked α-D-galacturonic acid (homogalacturonan, HG) or repeats of the disaccharide [→4)-α-D-GalA-(1→2)-α-L-Rha-(1→] (rhamnogalacturonan, RG) are elaborated with a range of modifications and substitutions. These include methyl-esterification, acetylation, and the addition of neutral polysaccharide side chains. Side chains may be attached to HG and RG to form the branched polysaccharides RG-II and RG-I, respectively, the latter often rich in (1→5)-α-L-arabinan and (1→4)-β-D-galactan components (O'Neill et al., 1990; Albersheim et al., 1996; Mohnen 1999). Several of these pectic structures appear to be capable of being enzymatically modified in muro. For example, the de-esterification of HG by pectin methyl esterases (PMEs) influences its capacity to form calcium cross-linked gels. The relationships of pectic polysaccharide domains within large polymer structures and their functional properties in relation to factors such as porosity, cell adhesion and expansion, ionic and hydration status, and cell signaling, are far from clear.

Ripening-related textural changes in the tomato (*Lycopersicon esculentum*) fruit pericarp have been extensively studied and are thought to be associated with alterations in CW properties due to modifications of the polysaccharide components, including the cellulose-xyloglucan network (Sakurai and Nevins, 1993; Maclachlan and Brady, 1994; Rose and Bennett, 1999) and the pectic matrix (Gross and Sams, 1984; Seymour et al., 1990). Several single-gene mutations have pleiotropic effects on ripening, including an inhibition of fruit softening, and these have been very useful for understanding the molecular mechanisms associated with softening (DellaPenna et al., 1989; Gray et al., 1994). A pleiotropic tomato ripening mutant, *Cnr* (colorless non-ripening), has recently

[1] This work was supported by the United Kingdom Biotechnology and Biological Sciences Research Council (G.B.S., A.J.T.), including a Co-operative Award in Science and Engineering studentship with Horticulture Research International (to C.O.) and a grant (no. 17/DC09694 to I.M.H.).

* Corresponding author; e-mail j.p.knox@leeds.ac.uk; fax 44–113–2333144.

been described with altered physical properties of the pericarp, including reduced cell-to-cell adhesion (Thompson et al., 1999). Although the genetic basis of this mutation has not yet been elucidated, it has been instructive to examine aspects of the CW in the pericarp of *Cnr* fruit to gain insights into processes involved in the ripening of tomato fruit. In this report we focus on the pectic polysaccharides of the CW matrix and the ML. We show that maturation processes involving ML HG are altered in *Cnr* fruit and result in reduced cell adhesion. Furthermore, we demonstrate that the deposition of (1→5)-α-L-arabinan is disrupted in *Cnr* fruit prior to ripening. This is likely to be a key factor underlying CW properties in the *Cnr* phenotype.

RESULTS

Altered CW Properties in *Cnr* Pericarp

To investigate the molecular basis of the textural properties of *Cnr* fruit, pericarp CW of cv Ailsa Craig wild type (WT) and the near-isogenic mutant *Cnr* from red-ripe (RR) stage fruit (about 60 d post-anthesis [DPA]) and mature-green (MG) fruit (about 40 DPA) were examined. Staining of sections of resin-embedded pericarp with the cellulose-binding probe Calcofluor White indicated that the cells walls in ripe WT fruit were thicker than the CW of *Cnr* fruit of an equivalent age, as shown in Figure 1. This was most apparent in the outer pericarp region of RR fruit where expanded ML can be seen (Fig. 1B). The reduction of cell-cell adhesion in *Cnr* fruit during the ripening process was greatest in the inner pericarp where large intercellular spaces were observed in *Cnr* (Fig. 1, G and H), but not in the WT (Fig. 1, E and F). Estimation from sections indicated that there was approximately 50% more intercellular space in *Cnr* pericarp than in WT. The larger intercellular air spaces in *Cnr* pericarp are likely to account for the observation that RR *Cnr* fruit (or excised pieces of pericarp) float when placed in water, whereas RR WT fruit sink (data not shown).

Different swelling capacities of isolated CW material (CWM) from WT and *Cnr* fruit were observed following suspension in water. During ripening, the volume of an equivalent weight of WT CW, when hydrated in vitro, increased approximately 4-fold, whereas CWM from *Cnr* fruit showed no increase (Fig. 2A). The CW swelling that occurs during the normal ripening process (Crookes and Grierson, 1983; Redgwell et al., 1997b) does not occur in *Cnr*

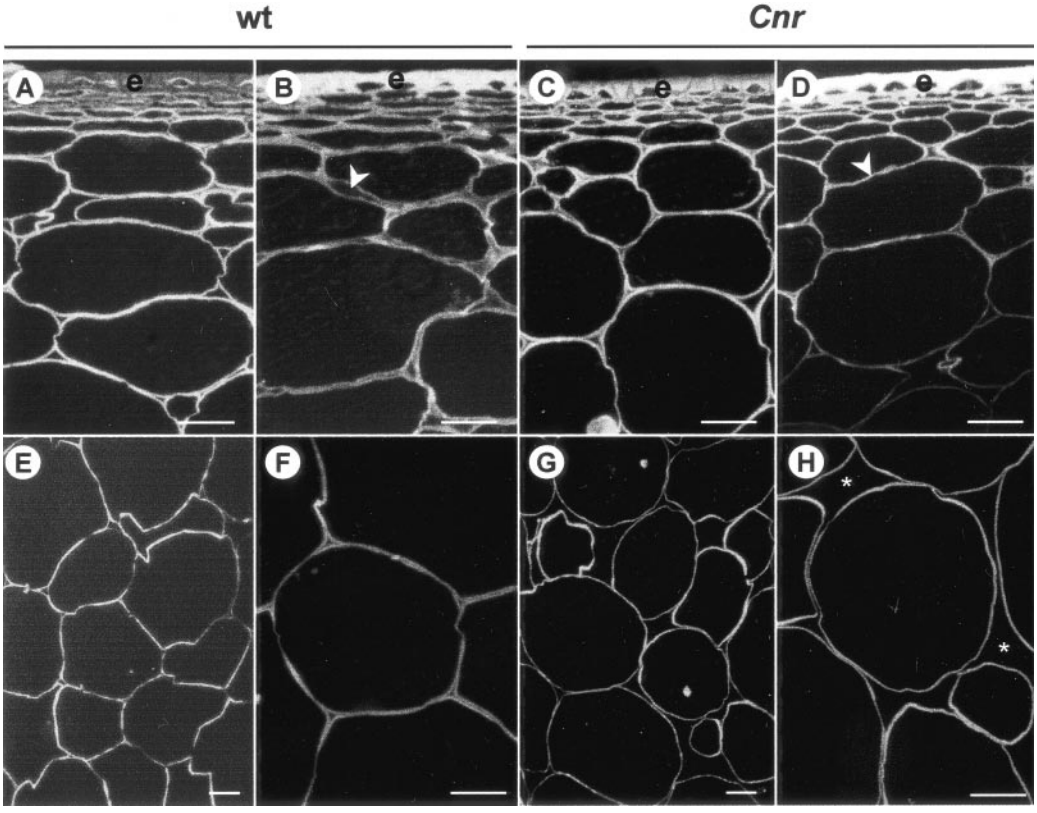

Figure 1. Calcofluor White staining of cellulose in resin-embedded sections of pericarp. A, Outer pericarp of MG WT fruit. B, Outer pericarp of RR WT fruit. Arrowhead indicates expanded ML. C, Outer pericarp of MG *Cnr* fruit. D, Outer pericarp of RR *Cnr* fruit. Arrowhead indicates compact cell walls. E and F, Regions of the inner pericarp of RR WT fruit. G and H, Regions of the inner pericarp of RR *Cnr* fruit. Asterisks indicate large intercellular spaces. e, Epidermis. Bars = 200 μm.

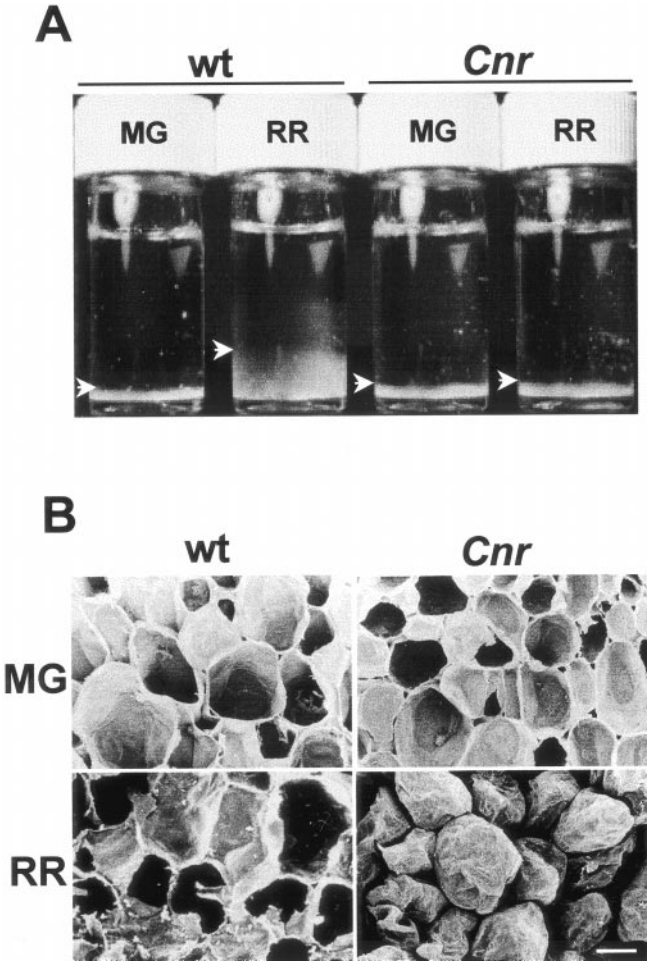

Figure 2. CW properties. A, CW swelling in vitro. Equivalent dry weights of isolated CWM from WT and *Cnr* pericarp at MG and RR stages were suspended in water and allowed to hydrate at room temperature for 8 h with gentle agitation then allowed to settle. CWM is seen at the base of each vial (arrowheads). B, Scanning electron micrographs of fracture surfaces of fruit pericarp of WT and Cnr at MG and RR stages. RR *Cnr* pericarp cells separate and do not rupture. Bar = 200 μm.

fruit and its CW and ML are more compact at the ripe stage.

Examination of fracture planes with a scanning electron microscope indicated distinct adhesion properties in *Cnr* fruit, as shown in Figure 2B. At the MG stage, *Cnr* pericarp cells ruptured in a manner equivalent to WT. In contrast, no cell rupture occurred in *Cnr* fruit at the RR stage, and the cells separated (Fig. 2B). This demonstrates that the increased capacity for cell separation of RR *Cnr* pericarp does not require the solubilization of any CW components, which may occur when CW separation studies are carried out in water (see below, Thompson et al., 1999). These observations provide further evidence that changes do occur in *Cnr* pericarp CW during ripening and that these changes result in stronger CW, weaker intercellular connections, or both of these factors.

To study the strength of CW, pericarp tissue was subjected to two types of mechanical analysis. One set of analyses involved the determination of the forces required for CW failure using a single-cell probe. The results (Fig. 3A) indicate that at the MG stage CW strength in *Cnr* is similar to that in WT. Although some loss of wall strength does occur during the ripening process, this is not as extensive in *Cnr* as in WT. The force required to induce CW failure drops by only approximately 25% in *Cnr*, compared with a reduction of approximately 80% in WT pericarp cells (Fig. 3A). In addition, compression stiffness modulus was used as a measure of tissue mechanical properties. *Cnr* pericarp had a significantly higher compression stiffness at the MG stage when compared with WT, and this declined during ripening by approximately 70% (Fig. 3B). In comparison, the compression stiffness modulus of pericarp

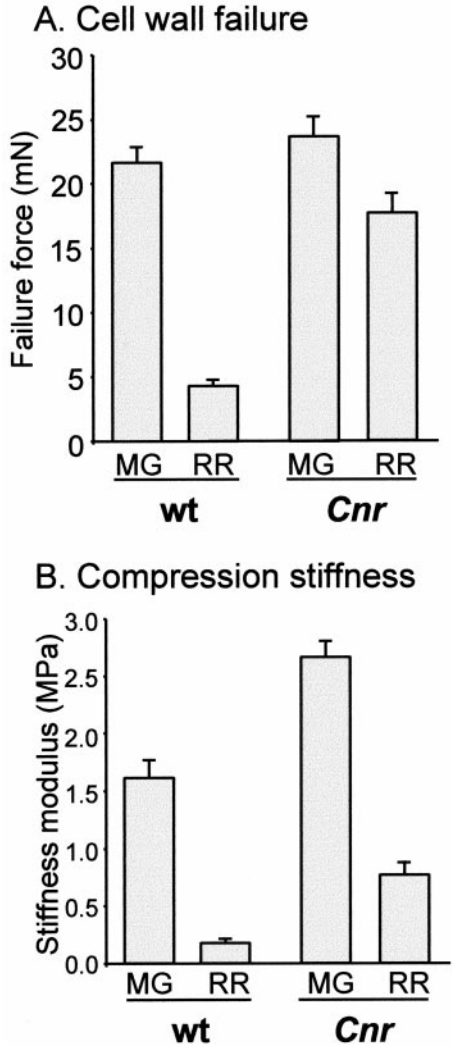

Figure 3. Mechanical analyses of pericarp material. A, Force required for CW failure in WT and *Cnr* MG and RR fruit. Error bars indicate SE of the mean (n = 6). B, Compression stiffness moduli for WT and *Cnr* MG and RR fruit. Error bars indicate SE of the mean (n = 6).

tissue from WT declined by approximately 90% (Fig. 3B), resulting in significantly reduced stiffness at the RR stage.

In summary, the pericarp of ripe *Cnr* has stronger, less swollen, less adherent CW than the WT pericarp at the ripe stage. Although the reduced cell adhesion characteristic of *Cnr* is manifest at the developmental stage equivalent to RR, it is of interest that a difference in compression stiffness was observed at the MG stage.

Compositional Analysis of Pericarp CW

Analysis of the monosaccharide composition of isolated CW from pericarp of *Cnr* and WT fruit indicated no major differences, although there was an indication of elevated levels of Gal in *Cnr* at the MG and RR stages (Table I). Determination of the level of methyl esterification of the galacturonan components in the CWM indicated similar levels and an equivalent decline during ripening in WT and *Cnr* fruit (Table I). These data indicate that the reduced CW swelling and reduced cell adhesion observed in *Cnr* pericarp are not due to a gross change in CW polysaccharide composition.

Maturation of Pericarp ML Is Disrupted in *Cnr* Fruit

In WT pericarp, cell-to-cell adhesion is known to be altered during the ripening process, and in ripe fruit cell-to-cell links are largely mediated by calcium cross-linking of de-esterified regions of HG, as evidenced by the capacity of calcium chelators to induce cell separation (Thompson et al., 1999). To study ML maturation in *Cnr* and WT pericarp the calcium-binding capacity of ML and primary CW at MG and RR stages was examined using electron energy loss spectroscopy (EELS), a method capable of measuring calcium-binding capacity at high resolution (Huxham et al., 1999). EELS analysis of resin-embedded material demonstrated that at the MG stage the CW and ML of *Cnr* pericarp had a significantly reduced capacity to bind calcium compared with WT, as shown in Figure 4. During ripening in the WT the CW shows a marked decrease in relative calcium-binding capacity, with a less marked change in the ML. In contrast, in *Cnr*, values for relative calcium binding in CW and ML are lower than for WT and increase slightly during ripening. Thus, the calcium-binding capacities of *Cnr* CW and ML are lower than WT prior to ripening and are not modified in the same way during ripening.

The pectic HG network of pericarp cells was examined by immunolabeling of resin-embedded sections with PAM1, a phage display monoclonal antibody specific to large stretches or blocks of de-esterified HG (Willats et al., 1999a). If PAM1 is used after sections have been treated to remove methyl ester groups, its binding indicates the presence of HG in CW independently of the extent or pattern of methyl esterification (Willats et al., 1999a). PAM1 labeling of resin-embedded sections of MG and RR pericarp of WT and *Cnr* indicated that the overall abundance of the PAM1 epitope on untreated sections was similar in WT and *Cnr*. However, there were distinctive spatial differences in the occurrence of the epitope at the ripe stage, as shown in Figure 5. In RR WT pericarp the PAM1 epitope was particularly abundant in the region of the CW lining intercellular spaces in untreated sections (Fig. 5A) and throughout the ML of chemically de-esterified sections (Fig. 5C). In contrast, the PAM1 epitope was not so abundant at the lining of intercellular spaces in *Cnr* and was generally absent from ML (Fig. 5B). Most significantly, this was even the case after de-esterification (Fig. 5D). In regions of the CW away from intercellular spaces, the PAM1 epitope was variable in its distribution and was generally absent from the ML. It was frequently observed to be absent from large areas stretching across adherent CW, as shown in Figure 5E. This was also apparent after chemical de-esterification of equivalent sections (Fig. 5F). However, some HG components were present in the ML of *Cnr* pericarp because the anti-HG probe JIM5 (that binds to a much smaller epitope than PAM1; Willats et al., 2001) bound to equivalent regions in serially related sections (Fig. 5, B, inset, and G).

An altered metabolism of pericarp HG during the ripening process in *Cnr* fruit was also reflected in water-soluble and calcium chelator-soluble pectic components. When pieces of pericarp were incubated in water and soluble material was analyzed by immunodot assay, the PAM1 epitope was considerably more abundant and a high-methyl-ester HG epitope

Table I. *Monosaccharide composition (molar percentage) and degree of esterification (DE) of uronic acids (UA; moles methanol per 100 moles UA) of isolated cell walls from WT and Cnr fruit at MG and RR stages*

Data are means of three analyses and values in parentheses are SE of the means.

	Monosaccharides							
	Rha	Ara	Xyl	Man	Gal	Glu	UA	DE
	% molar composition							
WT MG	3.62 (1.83)	5.82 (0.09)	5.35 (0.10)	4.95 (0.19)	11.02 (0.15)	33.57 (1.68)	35.31 (3.12)	80.23 (6.07)
Cnr MG	1.67 (1.66)	6.32 (0.50)	4.73 (0.03)	3.75 (0.13)	14.87 (2.70)	37.02 (2.70)	31.35 (3.67)	85.50 (4.76)
WT RR	1.60 (0.12)	6.07 (0.57)	6.45 (0.37)	6.02 (0.44)	5.11 (0.18)	26.40 (2.79)	48.35 (1.81)	46.60 (7.05)
Cnr RR	1.71 (0.13)	6.47 (0.35)	5.25 (0.35)	5.85 (0.57)	9.92 (0.75)	20.86 (4.59)	49.91 (5.88)	46.00 (4.43)

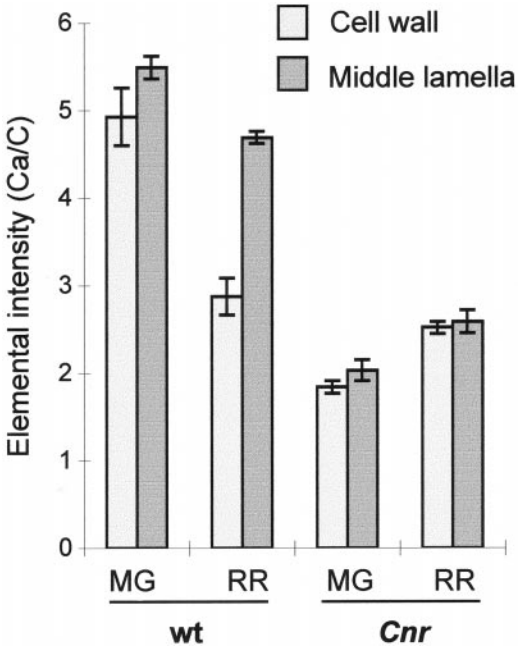

Figure 4. Calcium-binding capacity for WT and *Cnr* pericarp tissue at MG and RR developmental stages represented as the Ca/C elemental intensity ratios. Error bars indicate SEs of the mean.

(bound by JIM7) was less abundant in RR WT pericarp in comparison with material solubilized from *Cnr* pericarp (data not shown). This indicates that in *Cnr* fruit a water-soluble subset of HG components (that may derive from the ML and that would not be detected in the resin-embedded samples due to high solubility) was altered in the extent of its de-esterified block structure compared with WT. A range of de-esterified oligoglacturonides, analyzed by high-performance anion-exchange chromatography, were present in the calcium chelator-soluble fraction from WT RR pericarp, but absent from *Cnr* (data not shown), which is likely to reflect the absence of polygalacturonase (PG) expression in ripe *Cnr* fruit (Thompson et al., 1999).

Although the overall level of galacturonic acid and its methyl esterification are similar (Table I), EELS and analysis of HG components using antibody probes have indicated that significant differences exist in ML and soluble components of the HG network of ripe-stage *Cnr* when compared with WT. In short, although changes occur in the ML of *Cnr* pericarp CW during ripening as indicated by the EELS data, they do not result in the abundance of calcium cross-linkable HG capable of maintaining cell-to-cell adhesion seen in the WT.

Disrupted Deposition of (1→5)-α-Arabinan in *Cnr* Pericarp CW

To investigate other components of the pectic network, sections of resin-embedded pericarp material were probed with monoclonal antibodies to (1→5)-α-arabinan and (1→4)-β-galactan. These polysaccharide domains occur in side chains of RG-I (Albersheim et al., 1996; Mohnen, 1999). In MG pericarp of WT and *Cnr*, (1→4)-β-galactan occurred throughout the CW, but was generally absent from the ML and pit fields, as shown in Figure 6 and as previously reported (Jones et al., 1997; Orfila and Knox, 2000). In WT fruit pericarp the (1→5)-α-arabinan epitope also occurred evenly in CW and was absent from the ML (Fig. 6, C and D). In serially related sections of WT CW, it can be seen that the (1→5)-α-arabinan epitope appeared at a reduced level in regions of CW lining intercellular spaces in comparison with (1→4)-β-galactan (e.g. Fig. 6, B and D). Most significantly, the (1→5)-α-arabinan epitope did not occur in an equivalent manner in *Cnr* pericarp. In MG *Cnr* pericarp the (1→5)-α-arabinan occurred at a reduced level in the CW and was absent from an extended region of CW surrounding intercellular spaces. In addition, the (1→5)-α-arabinan epitope appeared to be abundant at the inner CW/plasma membrane and in vesicle-like structures in the peripheral cytoplasm (Fig. 6, H and I). This location of the (1→5)-α-arabinan epitope was consistent throughout the pericarp of *Cnr* fruit. The aberrant location was present at the MG stage and was even more apparent at the RR stage (Fig. 6J). The altered distribution of (1→5)-α-arabinan in *Cnr* pericarp was confirmed by immunogold electron microscopy of MG material. This indicated that the epitope was associated with vesicles in the peripheral cytoplasm in addition to some occurrence in the inner CW, near the plasma membrane, as shown in Figure 7. The deposition of (1→5)-α-arabinan appeared to be more disrupted in thinner regions of pericarp CW than in thicker regions.

The disrupted deposition of (1→5)-α-arabinan occurred in *Cnr* fruit, but was not seen in leaf or stem tissues of *Cnr* plants. Furthermore, immunolabeling of resin-embedded pericarp indicated that there was no equivalent alteration in the distribution of the (1→5)-α-arabinan epitope in the RR fruit of *rin* or *Never-ripe* non-ripening mutants (data not shown).

To explore the nature of the (1→5)-α-arabinan-containing material in *Cnr* fruit, SDS-PAGE analysis and immunoblotting using the LM6 antibody was performed. This indicated that a considerable amount of material carrying the (1→5)-α-arabinan epitope from MG *Cnr* entered the stacking and resolving SDS-PAGE gels, resulting in a high M_r smears, in contrast to WT (Fig. 8A). Loss of the LM6 reactivity after treatment with Pronase E prior to analysis indicated that the component entering the resolving gel was associated with protein (Fig. 8A). Figure 8B shows immunodot assays, using LM6, of the same preparations as used for SDS-PAGE analysis, indicating the presence of abundant (1→5)-α-arabinan-containing material in WT pericarp that did not enter the stacking or resolving gel systems.

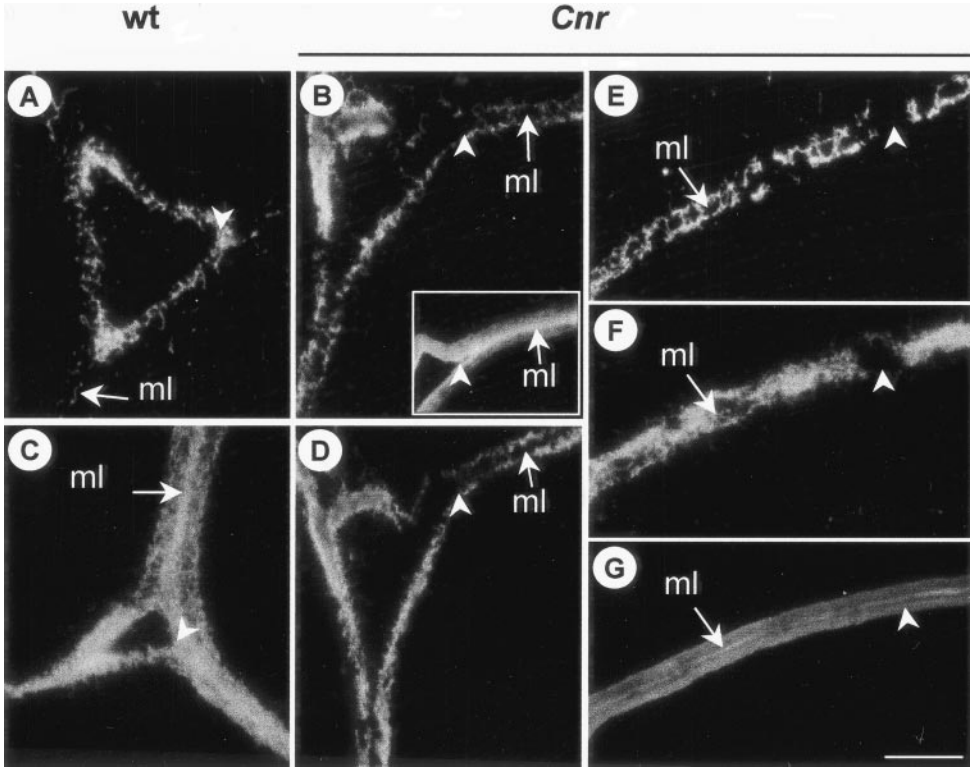

Figure 5. Immunolabeling of pectic HG components in regions of intercellular spaces in outer pericarp. A, Intercellular space of RR WT pericarp. The arrow indicates the ML. Arrowhead indicates abundant PAM1 labeling at corner of intercellular space. B, Intercellular space RR *Cnr* pericarp. Arrow indicates ML without PAM1 binding. Arrowhead indicates absence of PAM1 epitope from corner of space. Inset shows a serially related section of RR *Cnr* pericarp labeled with JIM5. C, Intercellular space of RR WT pericarp de-esterified before PAM1 probing. Arrow indicates abundance of PAM1 epitope at the ML. D, Intercellular space of RR *Cnr* pericarp de-esterified before PAM1 probing. Arrow indicates absence of PAM1 epitope from ML and corners of space. E and F, Region of CW away from intercellular space. The PAM1 epitope is absent from regions of the CW (arrowhead), even after de-esterification (F). G, Serially related section to E and F probed with JIM5 shows epitope throughout the CW and abundantly at the ML. In each case, arrow indicates ML. A through D, Arrowhead indicates corner of intercellular space. Bar = 5 μm for all micrographs.

DISCUSSION

Tomato fruit ripening involves the swelling and softening of CW and decreased cell adhesion, resulting in changes in fruit mechanical properties. In *Cnr*, CW swelling does not take place, CW are stronger, and cell adhesion is weakened significantly.

The bonds that maintain cell-to-cell contacts at the MG stage must be lost during the course of ripening (in *Cnr* and WT), as water or calcium chelators cannot induce cell separation at the MG stage (Thompson et al., 1999). From our EELS analysis, the calcium-binding capacity of the WT primary CW decreases markedly upon ripening, whereas that of the ML is maintained. In contrast, the relative calcium-binding capacity in *Cnr* was always lower than WT, with little difference between the ML and CW regions. The immunocytochemical studies indicate that the basis of the reduced calcium binding by *Cnr* ML is a modified pectic HG network and most notably the absence of long de-esterified stretches or blocks of HG recognized by PAM1. Although the precise structure of the *Cnr* ML HG is not known, it is clear that it cannot function in maintaining cell-to-cell attachment.

Modifications to the pectic network of the primary CW appear to be important for fruit softening during ripening, but they are poorly understood (Fischer and Bennett, 1991). Studies on pectins isolated from unripe tomato fruits have emphasized the importance of the polyelectrolyte and calcium-binding nature of pectin in promoting swelling (MacDougall et al., 1996; Tibbits et al., 1998). Studies have indicated that pectin solubilization occurs at early stages of fruit ripening (Seymour et al., 1990; Rose et al., 1998) and the swelling of CW in a range of fruit has been reported to correlate with pectin solubilization (Redgwell et al., 1997b). It has been reported previously that *Cnr* fruit do not express PG (Thompson et al., 1999) and preliminary evidence suggests that the activity of the main fruit-related isoform of PME in *Cnr* is reduced significantly (E. Eriksson, G. Tucker, and G.B. Seymour, personal communication). However, it is likely that PG and PME are just two of the

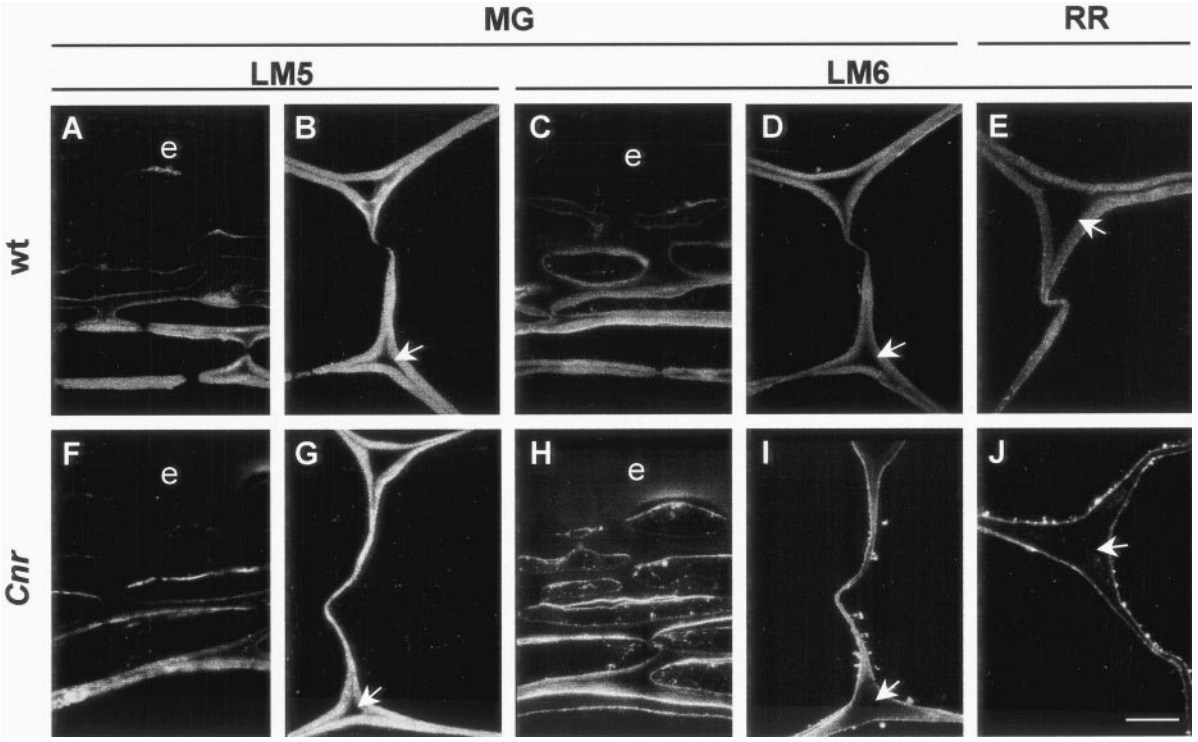

Figure 6. Immunofluorescent labeling of (1→4)-β-galactan and (1→5)-α-arabinan epitopes in tomato pericarp shows disrupted deposition of (1→5)-α-arabinan in *Cnr* fruit. A and B, The LM5 (1→4)-β-galactan epitope in resin-embedded sections of outer region of the pericarp (A) and inner pericarp CW (B) of MG WT fruit. C and D, The LM6 (1→5)-α-arabinan epitope in resin-embedded sections of outer region of the pericarp (C) and inner pericarp CW (D) of MG WT fruit. E, The LM6 (1→5)-α-arabinan epitope in resin-embedded sections of inner pericarp CW of RR WT fruit. F and G, The LM5 (1→4)-β-galactan epitope in resin-embedded sections of outer region of the pericarp (F) and inner pericarp CW (G) of MG *Cnr* fruit. H and I, The LM6 (1→5)-α-arabinan epitope in resin-embedded sections of outer region of the pericarp (H) and inner pericarp CW (I) of MG *Cnr* fruit. Throughout the pericarp the LM6 epitope occurs in vesicles located in the peripheral cytoplasm and in the inner region of the CW. J, The disruption of the LM6 (1→5)-α-arabinan epitope deposition and its absence from CW is particularly clear in the inner pericarp of RR WT fruit. Arrows indicate in each case the CW lining intercellular space. e, Epidermis. Bar = 10 μm.

many components that play a role in fruit softening. Transgenic tomato fruits with significantly reduced levels of PME activity have an increased level of pectin methyl esterification that correlated with reduced levels of bound calcium, but this had little impact on pericarp firmness during ripening (Tieman et al., 1992; Hall et al., 1993; Tieman and Handa, 1994). Furthermore, antisense reduction of PG mRNA in ripening tomato fruits did not disrupt softening (Smith et al., 1988; Carrington et al., 1993). The expression of PG in the *rin* mutant resulted in HG degradation, but not fruit softening (Giovannoni et al., 1989).

Taken overall, the observations indicate subtle alterations to the HG network in *Cnr*, and one consequence of this is reduced cell adhesion. It is not clear, however, how the alterations relate to other aspects of the *Cnr* phenotype. It is possible that pectic fragments generated during normal fruit ripening exert effects on cell physiology (Dumville and Fry, 2000) and that these factors are absent in *Cnr*. The relationship between the disrupted (1→5)-α-arabinan, the altered HG network, and altered CW properties are unknown. It is possible that (1→5)-α-arabinan has a direct role in CW swelling and its disrupted deposition in *Cnr* contributes to the lack of pericarp softening. Arabinans are known to be highly flexible, water-soluble polymers (Renard and Jarvis, 1999) and they may function directly in CW softening or by modulation of HG properties. Changes in Gal-containing polymers are well documented, and a decrease in Gal levels during ripening has been linked to fruit softening (Pressey, 1983; Gross and Sams, 1984; Seymour et al., 1990; Redgwell et al., 1997a; Rose et al., 1998). However, galactosidase activity is only detected after the onset of fruit softening (Carey et al., 1995; Smith et al., 1998). It is now apparent that (1→5)-α-arabinan and (1→4)-β-galactan are extensively modulated in CW in relation to CW architecture and cell development in a range of systems and thus are likely to have diverse functions (Jones et al., 1997; Willats et al., 1998, 1999b; McCartney et al., 2000; Orfila and Knox, 2000). For example, induction of cell elongation in a carrot cell culture correlates with up-regulation of (1→4)-β-galactan and decreased occurrence of (1→5)-α-arabinan (Willats et al., 1999b). The appearance of (1→4)-β-galactan in pea

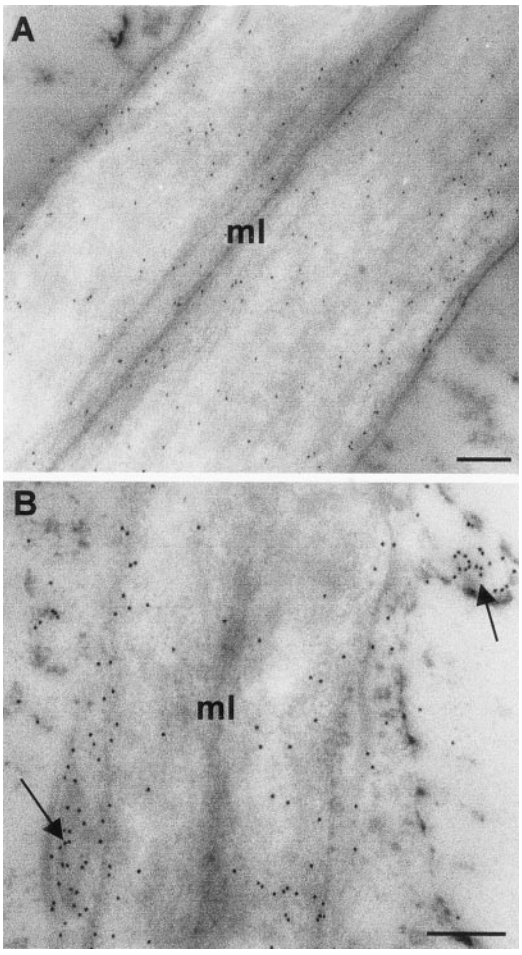

Figure 7. Immunogold electron microscopy of the (1→5)-α-arabinan epitope in MG tomato pericarp CW. A, In WT pericarp CW the LM6 (1→5)-α-arabinan epitope was evenly distributed. B, In *Cnr* pericarp CW the LM6 (1→5)-α-arabinan epitope occurred most abundantly at inner regions of the CW and was also associated with vesicle-like structures in the cytoplasm and at the plasma membrane (indicated by arrows). Bars = 200 nm.

cotyledons, relatively late in development, correlates with an increase in tissue firmness (McCartney et al., 2000). It may also be of significance that a greater compression stiffness modulus, reduced calcium-binding capacity, and the disrupted deposition of (1→5)-α-arabinan are all observed in MG stage *Cnr* fruit. It is known that some ripening-related changes start prior to ethylene-triggered ripening processes (Gillaspy et al., 1993; Thompson et al., 1999).

Evidence suggests that the (1→5)-α-arabinan epitope in *Cnr* is associated with protein. This may indicate that the epitope is carried by a glycoprotein or proteoglycan that is just at or below the level of detection due to a high turnover or incorporation into non-detergent-soluble fractions in WT fruit, but accumulates in *Cnr* fruit. One possibility is that the epitope is carried by a member of the arabinogalactan-protein (AGP) group of cell surface proteoglycans. AGPs are known to be a diverse and heterogeneous group (Nothnagel, 1997) and the presence of (1→5)-α-linked arabinosyl side chains has been reported (Mollard and Joseleau, 1994). However, the (1→5)-α-arabinan-carrying component in *Cnr* did not react with anti-AGP monoclonal antibody LM2 or the synthetic AGP-binding β-glucosyl Yariv reagent (data not shown). Furthermore, the build up of the (1→5)-α-arabinan epitope near the plasma membrane coincides with a reduced occurrence in the CW, suggesting the disruption of the major component of the CW with (1→5)-α-linked arabinosyl residues, which is likely to be a RG-I fraction. These observations suggest that attachment to a protein component may be an aspect of (1→5)-α-arabinan deposition or its assembly into the pectic matrix, although an artifactual association with protein cannot be ruled out. It may be of significance that (1→5)-α-arabinan-containing material from WT fruit did not enter the stacking gel during SDS-PAGE analysis, presumably due to it being part of a large polymeric structure.

To our knowledge, this is the first report of a mutation known to result in the specific disruption of the secretion and/or deposition of a plant CW component. This disruption is likely to be a key factor leading to the *Cnr* texture phenotype. Moreover, the disruption of arabinan deposition is specific to *Cnr* in

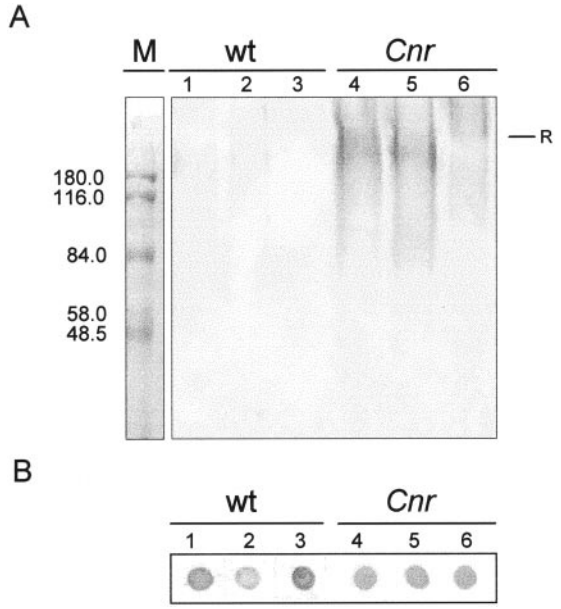

Figure 8. Immunochemistry of whole-cell extracts with anti-(1→5)-α-arabinan probe, LM6. A, Immunoblotting on nitrocellulose with LM6 of material separated by SDS-PAGE. Material (10 μg of protein per lane) from WT MG fruit (lanes 1–3) and *Cnr* MG fruit (lanes 4–6) were prepared in sample buffer immediately (lanes 1 and 4) or after incubation in Tris-buffer (lanes 2 and 5) or incubation in Tris-buffer plus Pronase E (lanes 3 and 6). Significant amounts of LM6-reactive, Pronase E-sensitive material entered the gel from *Cnr*, but not WT material. R indicates top of resolving gel. M shows M_r markers. B, Immunodot assay on nitrocellulose of material (0.4 μg of protein per dot) analyzed in A showing abundance of LM6 epitope in all samples.

that it does not occur in non-ripening *rin* or *Never-ripe* fruits. The observations also provide a basis for the further dissection of secretion mechanisms and CW assembly.

MATERIALS AND METHODS

Plant Material

Tomato (*Lycopersicon esculentum* Mill. cv Ailsa Craig) fruit and the mutant line *Cnr* in a cv Ailsa Craig background were grown in a heated greenhouse using standard cultural practices with regular additions of N,P,K fertilizer and supplementary lighting when required. The original mutant *Cnr* was detected in an F_1-hybrid cv Liberto (Thompson et al., 1999), and a homozygous mutant line was subsequently produced after selfing for four generations. This line was backcrossed to cv Ailsa Craig five times, and then selfed twice to produce a homozygous *Cnr* mutant line near-isogenic to cv Ailsa Craig. Plants were grown to three trusses. Fruits were harvested at the following stages: 20 DPA, MG, approximately 40 DPA; and RR, approximately 60 DPA. *Cnr* fruit do not become red, but were harvested at equivalent times to WT fruit and are designated RR in this report. Seeds for the *rin* and *Nr* ripening mutants were obtained from the Glasshouse Crops Research Institute collection at Horticulture Research International (Wellesbourne, UK).

Analysis of Mechanical Properties

Compression stiffness modulus was measured by axially loading pericarp tissue discs using an LRX materials testing machine (Lloyd Ltd., Fareham, Hampshire, UK) fitted with a 500 N load cell and controlled by Nexygen-Ondio 3.0 software. Fruit were sectioned so that tissue discs of 15 mm diameter could be excised with a cork borer from the equatorial region. Areas containing columellar tissue were avoided and placental tissue was removed. Two discs, from opposite sides, taken from each of three fruit per treatment were measured. The thickness of each tissue disc was measured using calipers, the disc was then compressed between parallel plates at 5 mm min^{-1}, and the stiffness modulus calculated from disc dimensions and the slope of the force/deformation curve (Jackman and Stanley, 1992).

CW strength was determined as the force required to penetrate the CW of individual cells with a 50-μm diameter flat-ended probe driven at 10 $\mu m\ s^{-1}$. Tissue was excised from the equatorial region and sectioned to produce a sample approximately 4 mm thick by 15 mm long with the width being determined by the thickness of the pericarp, so that the long axis of the sample was parallel to the pedicel to blossom end axis. The probe was driven into the tissue sample to a depth of 1.5 to 2 mm, such that the direction of travel was parallel to the skin. Measurements were carried out at six positions on one sample from each fruit used for the compression measurements and at each position the failure force for up to eight cells was recorded.

EELS

Duplicate samples of tomato tissue samples were placed into 70% (v/v) ethanol and were dehydrated using an alcohol series and then embedded in LR White resin for 2 d before polymerization using UV light. Light gold (60–80 nm thickness) sections were prepared from two locations for each group for EELS analysis (sampling: $2 \times 3 \times 2 = 12$ locations). Sections were doped with 5 mM calcium acetate for 1 h at room temperature and were washed three times with water before analysis. EELS analysis of undoped sections revealed no detectable calcium present. Analysis was carried out using a transmission electron microscope (902 Leo, Zeiss, Jena, Germany) operating at 80 KV, using a 60-μm objective aperture with a vacuum of 5×10^{-7} torr. All image sequences were recorded at 12,000× magnification using a 3 eV exit aperture containing nonoverlapping spectral images covering a range of the energy spectrum from 240 to 400 eV for the carbon and calcium ionization edges. Fourteen-bit, 1,024 × 1,024 pixel images were collected using a slow-scan cooled charge-coupled device camera (Proscan Elektronische Systeme, Scheuring, Germany) with fixed gain and bias by integration over 5,000 ms for each image. Two spectral ranges included electron energy loss information for both elements of interest: carbon (288 eV) and calcium (335 eV). For each sample 12 data sets were collected. Areas of interest were divided into the ML and the CW. Electron energy loss image sequences were analyzed using EsiVision and AnalySiS software specifically designed for EELS data by Zeiss/Leo. Integrated energy loss values per pixel for carbon and calcium were determined using the least mean squares fit of the Ae-r power law model of the immediate background of each spectrum by projection and subtraction. Data were calculated in terms of the relative intensity per unit area and summarized using EXCEL. The relative intensity values for carbon and calcium were measured and the relative intensity ratios for calcium/carbon (×100) calculated for each domain. This calculation accommodated any natural variation between the received electron dose and the section thickness from one sample to another.

Scanning Electron Microscopy

Tomato fruit were washed and the pericarp was cut into large cubes (1 cm^3). The cubes were frozen under liquid nitrogen and fractured using a pestle so that small fragments (approximately 0.03 cm^3) were obtained. The pericarp fragments were fixed in 2.5% (w/v) glutaraldehyde in 0.1 M sodium phosphate buffer, pH 7.2, for 2 h at 4°C, and then washed extensively with sodium phosphate buffer and subsequently post-fixed in 1% (w/v) osmium tetroxide in sodium phosphate buffer for 1 h at 4°C. The fragments were washed extensively in sodium phosphate buffer and dehydrated in an acetone series (10%–100%). Dehydrated fragments were critical-point dried, mounted onto metal studs, coated with colloidal gold, and viewed using a scanning electron microscope (CamScan, Leica, Cambridge, UK).

Preparation of Pericarp Tissue for Microscopy

Pericarp cubes (0.06 cm^3) were fixed in 2.5% (w/v) glutaraldehyde in 0.1 M sodium phosphate buffer, pH 7.2, for 2 h at 4°C, and then washed extensively with sodium phosphate buffer. Cubes were post-fixed in 1% (w/v) osmium tetroxide in 0.1 M sodium phosphate buffer for 1 h at 4°C, washed extensively with sodium phosphate buffer, and then dehydrated in an ethanol series (70%–100%). Dehydrated cubes were infiltrated with LR White resin (London Resin, Reading, UK), then placed in gelatin capsules containing LR White resin and allowed to polymerize at 37°C for 5 d.

Immuno- and Cytochemical Labeling for Light Microscopy

Antibody probes for HG included PAM1, a phage display monoclonal antibody that binds to large de-esterified blocks of HG (Willats et al., 1999a), JIM5, and JIM7 (Knox et al., 1990; Willats et al., 2001). Antibody probes for epitopes carried by RG-I included LM5 to (1→4)-β-D-galactan (Jones et al., 1997) and LM6 to (1→5)-α-L-arabinan (Willats et al., 1998).

Sections obtained from resin-embedded material (0.5-μm thickness) were incubated in a 5% (w/v) solution of fat-free milk powder in phosphate-buffered saline (PBS), pH 7.2, for 30 min. Sections were then incubated in a solution containing anti-HG PAM1 phage monoclonal antibody (approximately 10^{12} phage particles mL^{-1}) in milk powder/PBS for 1.5 h. The sections were then washed extensively with PBS and were post-fixed with 1% (w/v) glutaraldehyde in PBS for 10 min. The sections were washed extensively with PBS and then incubated with a solution containing mouse anti-M13 monoclonal antibody (Pharmacia, Uppsala) diluted 1:50 in milk powder/PBS for 1.5 h. The sections were extensively washed in milk powder/PBS and then incubated in a solution containing anti-mouse monoclonal antibody linked to fluorescein isothiocyanate (Sigma, St. Louis) diluted 1:100 in milk powder/PBS. The sections were washed extensively with PBS, mounted in a glycerol/PBS/fluorescence anti-fade solution (Citifluor AF3, Agar Scientific, Stansted, UK), and examined with a microscope equipped with epifluorescence. Where specified, sections were treated with 0.1 M Na_2CO_3 for 30 min to chemically de-esterify pectin, then washed extensively with deionized water. For cytochemical staining of cellulose, sections were treated with a solution of 0.025% (w/v) Calcofluor White (fluorescent brightener 28, Sigma) in deionized water for 30 s, then washed extensively with deionized water. Sections were mounted as described above and observed using a microscope equipped with UV fluorescence.

Preparation of Enzyme-Free CW

Isolation of CWM was based on a method described previously (Seymour et al., 1990). Fruit were washed, peeled, and the pericarp was cut into small cubes (0.125 cm^3), which were then homogenized in 4 volumes of acetone at −20°C using a homogenizer (Polytron, Kinematica, Lucerne, Switzerland). The homogenate was filtered through Miracloth (Calbiochem-Novabiochem, San Diego) and washed with 80% and 100% (w/v) acetone (12.5 mL g^{-1} tissue fresh weight). Acetone-insoluble solids were suspended in a solution of phenol:acetic acid:water (PAW, 2:1:1, w/v, 10 mL g^{-1} tissue fresh weight) and the mixture was stirred for 15 min at 4°C. After PAW treatment, acetone was added to a final concentration of 80% (v/v) and the mixture was filtered though a sintered glass filter. The filtrate was washed with 100% (w/v) acetone (200 mL) to remove traces of PAW. The obtained CWM was dried in air at room temperature (for CW hydration studies) or dried over P_2O_5. In both cases CWM was stored desiccated at −20°C.

The in vitro hydration of CW was visualized as follows. CW (3 mg dry weight) were suspended in 5 mL of water and allowed to hydrate for 8 h with gentle rocking at room temperature. CW were then allowed to sediment at 4°C for 30 min.

Determination of Total Monosaccharide Composition

Neutral monosaccharide composition was determined by gas liquid chromatography as described by Selvendran et al. (1979) with modifications by Blakeney et al. (1983). UA content was determined according to Blumenkrantz and Absoe-Hansen (1973) and the degree of methyl esterification was determined according to Wood and Siddiqui (1971), with minor modifications (addition of 0.1 M osmium tetroxide to the 0.125 M potassium permanganate solution and to the acidified 0.125 M arsenite solution).

SDS-PAGE and Immunoblotting

Tomato pericarp was frozen and ground to a fine powder using a mortar and pestle. The powder (2 mL) was suspended in 50 mM Tris-HCl, pH 6.5, or 50 mM Tris-HCl, pH 6.5, containing Pronase E (Sigma) at 1 mg mL^{-1}. Samples were vortexed and boiled for 5 min or left at room temperature for 2 h. All samples were then suspended in double-strength SDS-sample buffer, vortexed, and boiled for 5 min. Protein concentration of the samples were determined using a Bio-Rad (Hercules, CA; Bradford) protein assay. Aliquots containing 10 μg of protein were loaded per lane for SDS-PAGE analysis and immunoblotting with LM6 as described in Smallwood et al. (1996) and 1-μL aliquots (0.4 μg of protein) were directly assayed for LM6 binding by immunodot assays as described in Willats et al. (1999b). Anti-AGP monoclonal antibody LM2 and β-glucosyl Yariv reagent were also used to probe the blots as described previously (Smallwood et al., 1996).

Cell Separation and Isolation of Soluble Pectic Components

Pericarp was cut into small cubes (0.03 cm^3) and incubated in three volumes of deionized water or 0.1 M calcium chelator (cyclohexanediamine-*N*,*N*,*N*′,*N*′-tetraacetic acid), pH 6.5, at room temperature, with gentle rocking. After 3 h

the supernatant was collected, filtered though glass fiber, and analyzed by immunodot assays as described elsewhere (Willats et al., 2001), or ethanol was added to a concentration of 70% (w/v), carbohydrate and protein polymers were allowed to precipitate overnight at 4°C, and the solution was centrifuged (4,000 rpm) and the pellet was freeze-dried. The dry pellet was resuspended in deionized water to a concentration of 1 mg mL^{-1} and was analyzed by high performance anion-exchange chromatography as described elsewhere (Willats et al., 1999a).

Received November 2, 2000; returned for revision December 8, 2000; accepted February 6, 2001.

LITERATURE CITED

Albersheim P, Darvill AG, O'Neill MA, Schols HA, Voragen AGJ (1996) An hypothesis: the same six polysaccharides are components of the primary cell walls of all higher plants. *In* J Visser, AGJ Voragen, eds, Pectins and Pectinases. Elsevier Science, Amsterdam, pp 47–55

Blakeney AB, Harris PJ, Henry RJ, Stone BA (1983) A simple and rapid preparation of alditol acetates for monosaccharide analysis. Carbohydr Res **113:** 291–299

Blumenkrantz N, Absoe-Hansen G (1973) New method for quantitative determination of uronic acids. Anal Biochem **54:** 484–489

Brady CJ (1987) Fruit ripening. Annu Rev Plant Physiol **38:** 155–178

Carey AT, Holt K, Picard S, Wilde R, Tucker GA, Bird CR, Schuch W, Seymour GB (1995) Tomato exo-(1–4)-β-D-galactanase: isolation, changes during ripening in normal and mutant tomato fruit, and characterization of a related cDNA clone. Plant Physiol **108:** 1099–1107

Carrington CMS, Greve LC, Labavitch JM (1993) Cell-wall metabolism in ripening fruit: VI. Effect of the antisense polygalacturonase gene on cell wall changes accompanying ripening in transgenic tomatoes. Plant Physiol **103:** 429–434

Crookes PR, Grierson D (1983) Ultrastructure of tomato fruit ripening and the role of polygalacturonase isoenzymes in cell-wall degradation. Plant Physiol **172:** 1088–1093

DellaPenna D, Lincoln JE, Fisher RL, Bennett AB (1989) Transcriptional analysis of polygalacturonase and other ripening associated genes in Rutgers, *rin*, *nor* and *Nr* tomato fruit. Plant Physiol **90:** 1372–1377

Dumville JC, Fry SC (2000) Uronic acid-containing oligosaccharins: their biosynthesis, degradation and signalling roles in non-diseased plant tissues. Plant Physiol Biochem **38:** 125–140

Fischer RL, Bennett AB (1991) Role of cell wall hydrolases in fruit ripening. Annu Rev Plant Physiol Plant Mol Biol **42:** 675–703

Gillaspy G, Ben-David H, Gruissem W (1993) Fruits: a developmental perspective. Plant Cell **5:** 1439–1451

Giovannoni JJ, DellaPenna D, Bennet AB, Fisher RL (1989) Expression of a chimeric polygalacturonase gene in transgenic rin (ripening inhibitor) tomato fruit results in polyuronide degradation but not fruit softening. Plant Cell **1:** 52–63

Gray JE, Picton S, Giovannoni JJ, Grierson D (1994) The use of transgenic and naturally occurring mutant to understand and manipulate tomato fruit ripening. Plant Cell Environ **17:** 557–571

Gross KC, Sams CE (1984) Changes in cell wall neutral sugar composition during fruit ripening: a species survey. Phytochemistry **23:** 2457–2461

Hall LN, Tucker GA, Smith CJS, Watson CF, Seymour GB, Bundick Y, Boniwell JM, Fletcher JD, Ray JA, Schuch W et al. (1993) Antisense inhibition of pectin esterase gene expression in transgenic tomatoes. Plant J **3:** 121–129

Huxham IM, Jarvis MC, Shakespeare L, Dover CJ, Knox JP, Seymour GB (1999) Electron energy loss spectroscopic imaging of calcium and nitrogen in the cell walls of apple fruits. Planta **208:** 438–443

Jackman RL, Stanley DW (1992) Area- and perimeter-dependent properties and failure of mature-green and red-ripe tomato pericarp tissue. J Texture Studies **23:** 461–474

Jarvis MC (1984) Structure and properties of pectin gels in plant cell walls. Plant Cell Environ **7:** 153–164

Jones L, Seymour GB, Knox JP (1997) Localization of pectic galactan in tomato cell walls using a monoclonal antibody specific to (1→4)-β-D-galactan. Plant Physiol **113:** 1405–1412

Knox JP, Linstead PJ, King J, Cooper C, Roberts K (1990) Pectin esterification is spatially regulated both within cell walls and between developing tissues of root apices. Planta **181:** 512–521

MacDougall AJ, Needs PW, Rigby NM, Ring SG (1996) Calcium gelation of pectic polysaccharides isolated from unripe tomato. Carbohydr Res **923:** 235–249

Maclachlan G, Brady CJ (1994) Endo-1–4-beta-glucanase, xyloglucanase, and xyloglucan endo-transglycosylase activities versus potential substrates in ripening tomatoes. Plant Physiol **105:** 965–974

McCartney L, Ormerod AP, Gidley MJ, Knox JP (2000) Temporal and spatial regulation of pectic (1→4)-β-D-galactan in cell walls of developing pea cotyledons: implications for mechanical properties. Plant J **22:** 105–113

Mohnen D (1999) Biosynthesis of pectins and galactomannans. *In* D Barton, K Nakanishi, O Meth-Cohn, eds, Comprehensive Natural Products Chemistry, Vol 3. Elsevier Science, Amsterdam, pp 497–527

Mollard A, Joseleau J-P (1994) *Acacia senegal* cells cultured in suspension secrete a hydroxyproline-deficient arabinogalactan-protein. Plant Physiol Biochem **32:** 703–709

Nothnagel E (1997) Proteoglycans and related components in plant cells. Int Rev Cytol **174:** 195–291

O'Neill MA, Albersheim P, Darvill AG (1990) The pectic polysaccharides of primary cell walls. *In* PM Dey, ed, Methods in Plant Biochemistry, Vol 2. Academic Press, London, pp 415–441

Orfila C, Knox JP (2000) Spatial regulation of pectic polysaccharides in relation to pit fields in cell walls of tomato fruit pericarp. Plant Physiol **122:** 775–781

Pressey R (1983) β-Galactosidases in ripening tomatoes. Plant Physiol **71:** 132–135

Redgwell J, Fisher M, Kendal E, MacRae EA (1997a) Galactose loss and fruit ripening: high-molecular-weight

arabinogalactans in the pectic polysaccharides of fruit cell walls. Planta **203:** 174–181

Redgwell RJ, MacRae EA, Hallett I, Fischer M, Perry J, Harker R (1997b) In vivo and in vitro swelling of cell walls during fruit ripening. Planta **203:** 162–173

Renard CMGC, Jarvis MC (1999) A cross-polarization, magic-angle-spinning, ^{13}C-nuclear-magnetic-resonance study of polysaccharides in sugar beet cell walls. Plant Physiol **119:** 1315–1322

Rose JKC, Bennett AB (1999) Cooperative disassembly of the cellulose-xyloglucan network of plant cell walls: parallels between cell expansion and fruit ripening. Trends Plant Sci **4:** 176–183

Rose JKC, Hadfield KA, Labavitch JM, Bennett AB (1998) Temporal sequence of cell wall disassembly in rapidly ripening melon fruit. Plant Physiol **117:** 345–361

Sakurai N, Nevins DJ (1993) Changes in physical properties and cell wall polysaccharides of tomato (*Lycopersicon esculentum*) pericarp tissues. Physiol Plant **89:** 681–686

Selvendran RR, March JF, Ring SG (1979) Determination of aldoses and uronic acid content of vegetable fiber. Anal Biochem **96:** 282–292

Seymour GB, Colquhoun IJ, DuPont MS, Parsley KR, Selvendran RR (1990) Composition and structural features of cell wall polysaccharides from tomato fruits. Phytochemistry **29:** 725–731

Smallwood M, Yates EA, Willats WGT, Martin H, Knox JP (1996) Immunochemical comparison of membrane-associated and secreted arabinogalactan-proteins in rice and carrot. Planta **198:** 452–459

Smith CJS, Watson CF, Ray I, Bird CR, Morris PC, Schuch W, Grierson D (1988) Antisense RNA inhibition of polygalacturonase gene-expression in transgenic tomatoes. Nature **334:** 724–726

Smith DL, Starret DA, Gross KC (1998) A gene coding for the tomato fruit β-galactosidase II is expressed during fruit ripening. Plant Physiol **117:** 417–423

Thompson AJ, Tor M, Barry CS, Vrebalov J, Orfila C, Jarvis MC, Giovannoni JJ, Grierson D, Seymour GB (1999) Molecular and genetic characterization of a novel pleiotropic tomato-ripening mutant. Plant Physiol **120:** 383–389

Tibbits CW, MacDougall AJ, Ring SG (1998) Calcium binding and swelling behavior of a high methoxyl pectin gel. Carbohydr Res **310:** 101–107

Tieman DM, Handa AK (1994) Reduction in pectin methylesterase activity modifies tissue integrity and cation levels in ripening tomato (*Lycopersicon esculentum* Mill.) fruits. Plant Physiol **106:** 429–436

Tieman DM, Harriman RW, Ramamohan G, Handa AK (1992) An antisense pectin methylesterase gene alters pectin chemistry and soluble solids in tomato fruit. Plant Cell **4:** 667–697

Willats WGT, Gilmartin PM, Mikkelsen JD, Knox JP (1999a) Cell wall antibodies without immunisation: generation and use of de-esterified homogalacturonan block-specific antibodies from a naive phage display library. Plant J **18:** 57–66

Willats WGT, Limberg G, Bucholt HC, van Alebeek GJ, Benen J, Christensen TMIE, Visser J, Voragen A, Mikkelsen JD, Knox JP (2000) Analysis of pectic epitopes recognised by conventional and phage display monoclonal antibodies using defined oligosaccharides, polysaccharides and enzymatic degradation. Carbohydr Res **327:** 309–320

Willats WGT, Marcus SE, Knox JP (1998) Generation of a monoclonal antibody specific to (1→5)-α-L-arabinan. Carbohydr Res **308:** 149–152

Willats WGT, Steele-King CG, Marcus SE, Knox JP (1999b) Side chains of pectic polysaccharides are regulated in relation to cell proliferation and cell differentiation. Plant J **20:** 619–628

Wood PJ, Siddiqui IR (1971) Determination of methanol and its application to measurement of pectin ester content and pectin esterase activity. Anal Biochem **39:** 418–428